Optical Tweezer

Jaewon Jung[1]
[1] *Department of Physics and Astronomy, Seoul National University, Seoul 08858 Korea*

The unique technique, the optical tweezer, of manipulation and trapping of small particles is employed in this experiment. The 658 nm laser and micrometers scale polystyrene beads are used to observe a Brownian motion and measure trapping forces. The viscosity η are measured as 1.904 ± 0.0109 mPa·s, 1.322 ± 0.0060 mPa·s, and $1.670\ 0.0093 \pm$ mPa·s for 0.75 μm, 2 μm, and 3 μm beads. The trapping forces are measured as in the order of pN. Statistical analysis such as Gaussian fitting, Q-Q plot, and Hurst exponents calculation are done to verify if the observed Brownian motions are indeed ideal Brownian motion or not.

I. INTRODUCTION

Optical tweezer is a device based on highly focused light that can manipulate, trap, or characterize objects ranging from nanoscopic to microscopic. Using the Gaussian-shaped laser and assuming the spherical-shaped particles which are much bigger than the wavelength of the laser, the trapping force induced from the optical tweezer is considered as a gradient force or restoring force which is proportional to the laser intensity. Due to its powerful capability of manipulating small particles, it is widely used such as in biology, quantum optics, nanoengineering, and quantum optics.

In this report, we observe and measure the Brownian motion of the silica beads and numerically calculate the viscosity of the beads. Furthermore, we measure the trapping force of the optical tweezer by measuring the maximum velocity of the stage that can barely hold the beads. Then, we discuss and analyze the results of Brownian motion and trapping force obtained from the silica beads of three different diameters, 0.75 μm, 2 μm, and 3 μm.

A. Drag force

Drag force on spherical objects in a viscous fluid, is described by Stoke's law, as below [1].

$$F_d = 6\pi\eta R v, \tag{1}$$

where F_d is a drag force, η is viscosity, R is a radius of the spherical object and v is a flow velocity. Stoke's law gives a linear order of drag force compared to the quadratic drag force defined as in Eq. 2.

$$F_d = \frac{1}{2}\rho v^2 C A, \tag{2}$$

where ρ is fluid's density, v is a fluid velocity, C and A are drag coefficient and the cross-sectional area. The former gives the drag force dominated by viscous force while the latter gives the one dominated by inertia force which can be predicted by Reynolds number. Reynolds number is by definition a ratio between inertia and viscous forces in fluid dynamics. Therefore, if the Reynolds number is large, the inertia force (Eq. 2) dominates the drag force, in contrast, if the Reynolds number is relatively small, the viscous force (Eq. 1) dominates the drag force and accordingly, the drag force is mainly follows the Stoke's law. In principle, on the other hand, drag force can be defined by Taylor expansion of $F_d(v)$ and subsequently the linear term in this series represents the viscous force. Thus, it can be said that Stoke's law is valid when the fluid velocity is small enough.

In the case of silica beads in the experiment, Reynolds number is sufficiently small that the equation of motion is dominated by Stoke's law.

B. Optical tweezer

TEM_{00} mode Gaussian beam is primarily used for the optical tweezer. When this beam is incident to the bead, two different types of forces occur, the scattering and gradient force. When the gradient force is sufficiently greater than the scattering force, the particle can be trapped and this is determined by various factors such as bead size, focus position of the laser, and the viscosity of the fluid.

Rayleigh scattering regime $R \ll \lambda$

When the radius of the bead is significantly smaller than the wavelength of the incident laser, the force exerted by the laser can be described as gradient force induced by the electric dipole. Since the bead is assumed as dielectric, it can be considered that the bead is composed of N point dipoles, and the corresponding energy density of the bead is described as below.

$$U = \frac{N}{V}\left(-\vec{p}\cdot\vec{E}\right) = -\vec{P}\cdot\vec{E}, \qquad (3)$$

where $\vec{p}$ is a point dipole moment, $\vec{E}$ is the electrical field, V is a volume of the bead, and $\vec{P}$ is a polarization. Using above energy density, gradient force can be calculated and the force exerted on the bead is proportional to this gradient force.

$$F_{grad} = \frac{2\pi\alpha}{cn_m^2}\nabla I,$$
$$\alpha = n_m^2 R^3\left(\frac{m^2-1}{m^2+2}\right), m = \frac{n_p}{n_m} \qquad (4)$$

where α is the polarizability of the dipoles, n_m is the refraction index of the surrounding material, n_p is the refraction index of the bead, and ∇I is the intensity gradient. The scattering force is as below.

$$F_{scattering} = \frac{\sigma n_m}{c} I,$$
$$\sigma = \frac{128\pi^5 R^6}{3\lambda^4}\left(\frac{m^2-1}{m^2+2}\right)^2 \qquad (5)$$

where σ is the scattering cross-section. When the scattering force, or destabilizing force, is smaller than the gradient force, the stable trapping of the bead can be achieved.

Ray optics in the Mie regime $R \gg \lambda$

In contrast, if the radius of the bead is significantly larger than the wavelength of the incident laser, ray optics can be applied to describe the force exerted on the bead. In this regime, the particle nature of the light gets important and the force exerted on the bead can be derived from the momentum of the incident light. As shown in Fig. 1, the force can be divided into parallel and perpendicular direction to the incident beam and corresponding dimensionless Q factors which are proportional to the force is as below.

$$Q_s = 1 + R_r\cos(2\theta) - \frac{T^2(\cos(2\theta-2t)+R_r\cos(2\theta))}{1+R_r^2+2R_r\cos(2t)}$$
$$Q_g = R_r\sin(2\theta) - \frac{T^2(\sin(2\theta-2t)+R_r\cos(2\theta))}{1+R_r^2+2R_r\cos(2t)}$$
$$F_{s,g} = \frac{n_m P_{beam}}{c} Q_{s,g}, \qquad (6-8)$$

where $Q_s(Q_g)$ represents Q factor which contribute to the parallel(perpendicular) to the beam and R_r is a radius of the bead.

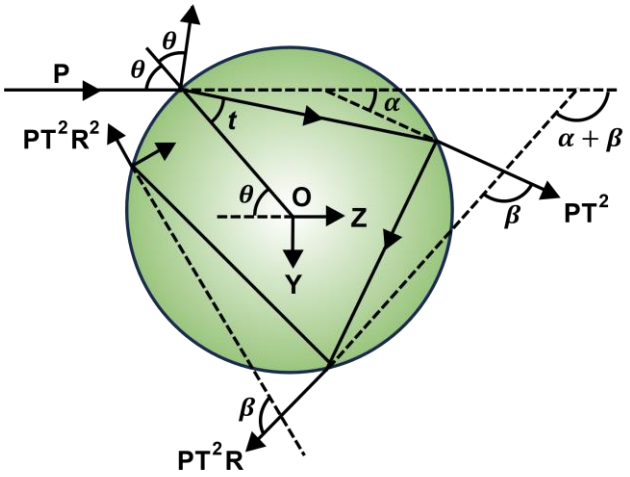

FIG. 1. The reflection (R) and transmission (T) of the incident beam (P) on the bead [2]. θ is an incident angle, t is a reflected angle, and α, β are angles that represent several reflected and transmitted beams.

C. Brownian motion

Brownian motion is the stochastic vibrating motion of the microscopic particle in the medium. The particle constantly collides with the surrounding molecules with random velocities that the particle suffers from random vibration as illustrated in Fig. 2. There are conditions for the stochastic process $B = \{B(t): t > 0\}$ to be defined as Brownian motion and are described below.

(1) $B(0) = 0$.
(2) The increments of B are independent and have normal distribution.
(3) B has continuous paths.

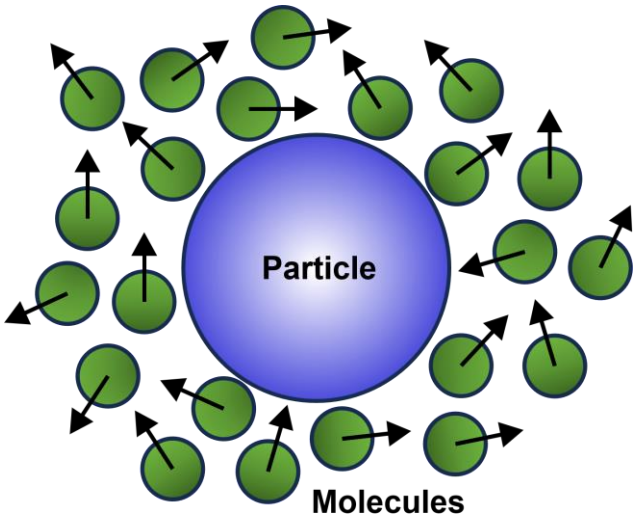

FIG. 2. A Brownian particle surrounded by molecules with random velocities.

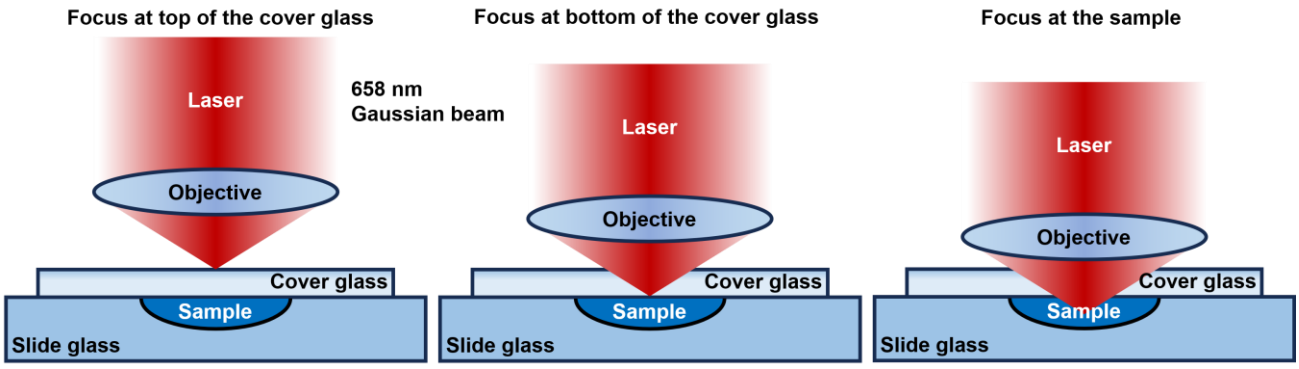

FIG. 3. Three different focus level of 658 nm Gaussian beam.

Brownian motion is a random process but still the ensemble average of the position can be predicted by Langevin equation. For simplicity, we consider 1D Brownian motion.

$$m\frac{d^2x}{dt^2} + \mu\frac{dx}{dt} = F, \tag{9}$$

$$< F_i(t)F_j(t') \geq 2k_B T\delta_{i,j}\delta(t-t'), \tag{10}$$

where m is the mass of the particle, μ is a damping coefficient, and F is the random force exerted on the particle which follows Gaussian distribution with correlation function in Eq. 10. As a result of Eq. 9, the time derivative of the ensemble average of the square of the position is described below.

$$g(t) = \frac{k_B T}{\mu}\left(1 - e^{-\frac{\mu}{m}t}\right), \qquad g(t) \equiv < x\frac{dx}{dt} > \tag{11}$$

where T is a temperature, and $\mu = 6\pi\eta R$ for the spherical bead. By the equipartition theorem, the coefficient of $g(t)$ gets two or three times in 2D and 3D, respectively.

$$\tau = \frac{m}{\mu} \sim \frac{1.05\ \frac{\mathrm{g}}{\mathrm{cm}^3}}{6\pi \cdot 1\ \mathrm{mPa \cdot s} \cdot 1\ \mu\mathrm{m}} \cdot \frac{4\pi}{3} \cdot 1\ \mu\mathrm{m}^3 \approx 0.23\ \mu\mathrm{s} \tag{12}$$

Characteristic time τ of a bead with radius 1 μm, viscosity 1 mPa· s, and density 1.05 g/cm^3 is in the order of μs that the mean squared displacement can be assumed to have linear relationship throughout the measurement time.

II. METHODS

The optical tweezer experiment is done using Thorlabs' portable optical tweezers educational kit [2]. For the laser source, 658 nm with 40 mW laser diode is used. Control of the stage and laser source is done by Thorlabs' kinesis software [3]. The beads used in this experiment are standard monodisperse polystyrene microspheres with nominal diameters 0.75 μm, 2 μm, and 3 μm [4]. The diameter of 0.75 μm microspheres range from 0.675-0.825 μm, 2 μm ranges from 1.80-2.20 μm, and 3 μm ranges from 3.00-3.30 μm. The density of the bead is around 1.05 g/cm^3 [5].

Sample preparation

To accurately measure the Brownian motion of the beads and the trapping force of the laser, making a good sample is critical since a poorly made sample significantly suffers from fast drift and external gradient force from bubbles. The procedure for preparing the sample is as follows.

1. Put deionized water of around 15~20 ml in the beaker.
2. Put 1-2 drops of the beads solution into the beaker using a pipette.
3. Put 1 drop of the dilute solution from above on the slide glass and cover with the cover glass carefully to minimize the creation of bubbles.
4. Load the slide glass on the stage carefully and observe how much of beads are in the unit cell and identify if there exists significant drift or not.
5. If the drift is large, adjust the amounts of drops and repeat the 3-4 process. If the drift is small enough, proceed to conduct the experiments.

Laser focusing

When the sample is ready from the previous section, using the kinesis software, turn on the laser and slowly move the stage up while observing three transitions of the laser point being visible and disappearing in the camera screen.

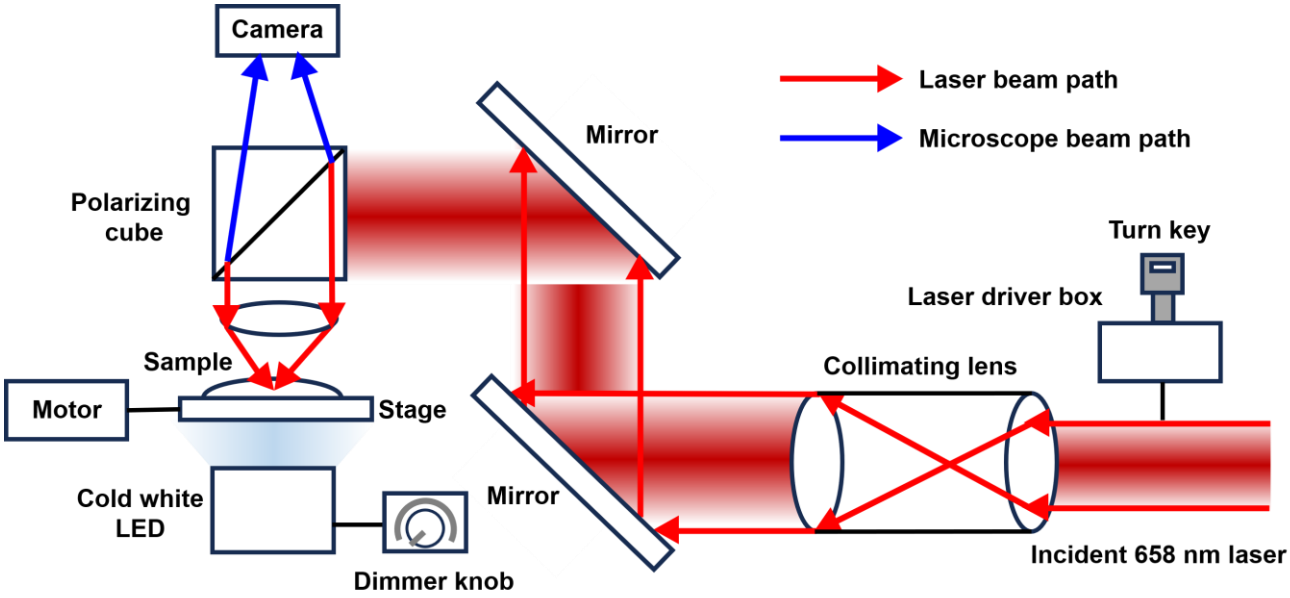

FIG. 4. Schematic of the optical tweezer kit setup. Red and blue lines indicate beam path of laser and microscope beam.

Around the third focus, be extra aware when raising the stage to avoid the crash of the lens. The laser point appears when the focus of the laser is at the upper and lower boundaries of the cover glass and the sample as illustrated in Fig. 3. When the laser is focused on the sample, verify if the laser is well focused on the sample by trying trapping the beads. If the beads are trapped around the laser points, the laser is ready for the experiments.

Brownian motion

From the Brownian motion, we can obtain the viscosity of the fluid by ensemble averaging the square of the position. The procedure is as follows.

1. Find the good spot that has clean background in the sample.
2. By using the optical tweezer aligned in the laser focusing part, trap the beads around 4 to 6 and move them to the good spot with sufficient spacing between each other. By using the sampled beads with the optical tweezer, we can assume those beads are in the same plane in the sample.
3. Turn off the laser and record the Brownian motion of the collected beads.
4. Utilizing the fixed beads or points in the sample, measure the standard distances in the x, y direction. From the measured distances, construct coordinate transformation matrix.
5. Using the tracker program, obtain the position vectors according to the time frames and calculate ensemble average of the square of the position vectors. Use obtained transformation matrix from above to accurately set the standard distance.

Trapping force measurement

Now, we measure trapping force of the laser. When we move the stage while one of the beads are trapped by laser, the frictional force and the trapping force compete on the beads. Thus, the trapping force can be obtained by the Eq. 1. By adjusting the input current of the laser and measuring the maximum velocity of the stage that can trap the beads, we can calculate the trapping force using Eq. 12 and cutoff current of the laser.

$$m = \frac{2k_B T}{3\pi\eta_{eff} R}, \tag{13}$$

where m is a gradient of the mean squared displacement of the beads.

For estimating the cutoff current of the laser, we utilize the linear relationship between trapping force and the power of the laser. The power of the laser also has linear relationship with the input current when the lasing is in steady state. Therefore, by finding when this linear relationship is violated in the trapping force versus input current data, we can estimate the threshold current.

III. RESULTS

The temperature was measured around 24 ℃ throughout the experiment. The number of beads measured in the experiments are 4, 5, 5 for 0.75 μm, 2 μm, and 3 μm.

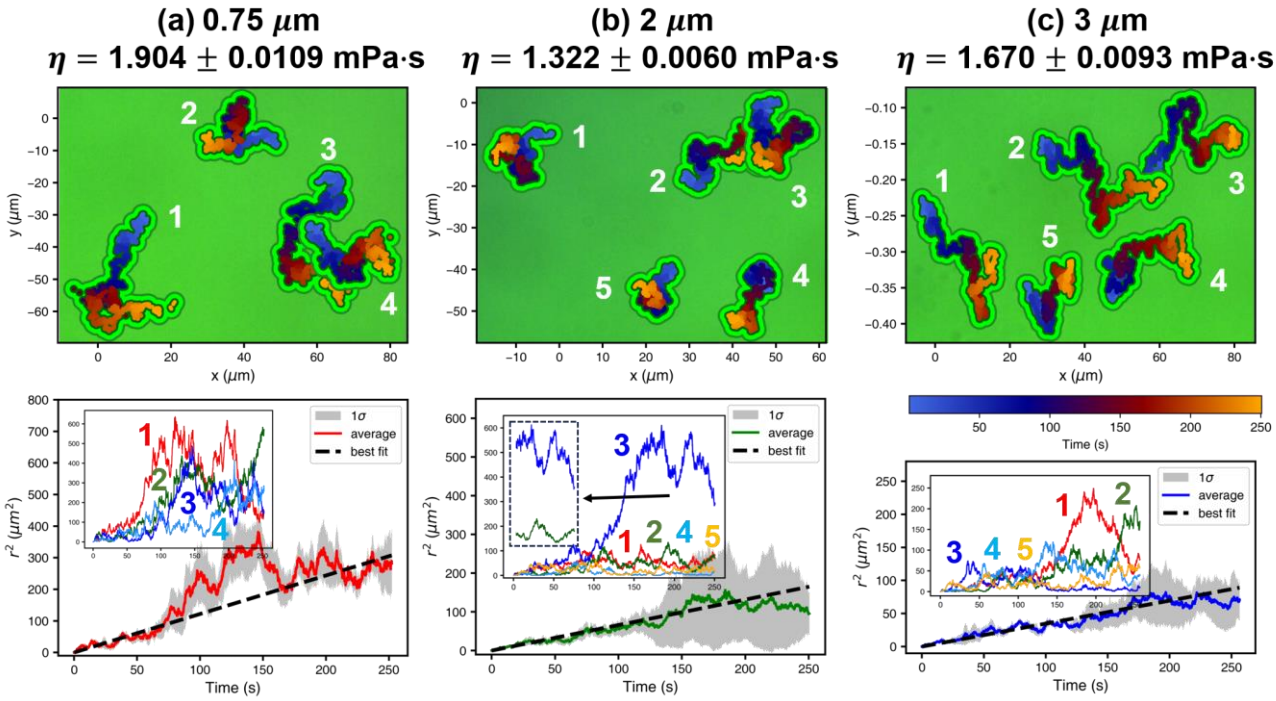

FIG. 5. The measured Brownian motion of 0.75 μm, 2 μm, 3 μm beads and corresponding mean squared displacement with corrections of drift velocities. The color bar represents time traces of the data. The insets in the lower plots show individual results of each particle. The dashed box in (b) indicates when the correlated movements happened between number 2 and 3 particles.

Brownian motion

From the results, the drift velocity is subtracted to obtain mean squared displacement, and 1σ ranges are obtained using a bootstrapping technique [6] which is a statistical technique that can estimate the effect of finite samplings. In this experiment setting, due to the limit of the size of the camera, it is challenging to capture more than 5 particles in a single measurement and each measurement takes about 4 minutes with additional sample preparation time that measuring plenty of particles' Brownian motion is practically demanding. Therefore, 1000 data points are sampled using bootstrapping and the variances are estimated using the sampled data.

In the calculation of the viscosity, the radii of the beads are assumed to be same as the labeled data though they have around 10 % standard deviation with respect to the mean value. The linear regressions are done using the 1σ ranges obtained from the bootstrapped data to compensate the inaccuracy induced from finite samplings. The measured viscosities are around 1.5 mPa·s with standard deviation less than 1 %. The measured values are consistent with theoretically predicted values.

From the inset in Fig. 5 (b), around t = 200 s, the number 2 and 3 particles got closer due to the electrostatic force which leads to adhesion and showed correlated movements that after t = 200 s, which can be the possible cause of deviation from linearity of the ensemble average of the mean squared displacement. In addition, the result of 0.75 μm beads showed high deviation from linearity compared to other radii results. One possible cause is lack of particle numbers than the others and the other cause is the presence of the interaction between number 3 and 4 particles around t = 150 s.

Trapping force

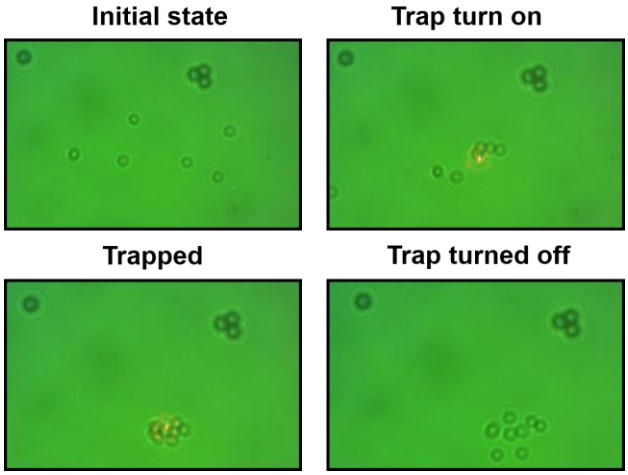

FIG. 6. Demonstration of trapping beads. The optical tweezer is used to gather the beads and the whole beads are trapped using laser.

When measuring the maximum holding force, the presence of the bubbles shown in Fig. 7 also affects the beads in the attracting way that the pathway of the measurement is carefully chosen.

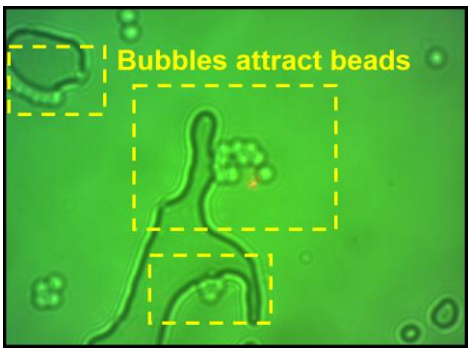

FIG. 7. Beads trapped near bubbles.

While measuring the trapping force, when the current is below 35 mA, starting from 30 mA, the optical trap did not work for beads which indicates that the threshold current is around 30 mA. Therefore, the laser power is calculated assuming the linear relationship between power and current considering the power is 40 mW at an operating current of 75 mA with a threshold current of 30 mA. The measured trapping forces are in the order of pN. The fluctuations in trapping force though low standard deviations are due to the inhomogeneity of the fluids. The measurement of trapping force is done with the integration time around 2 ~ 3 s and this corresponds to 0 ~ 2 mm in the sample. Along this range, the beads meet the other beads and also the concentration of the fluid differs that those are the main causes of the inaccuracies in the results.

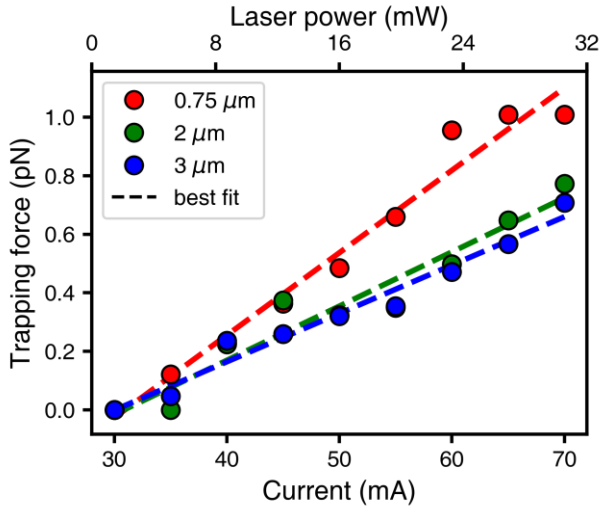

FIG. 8. The measured trapping force of 0.75 μm, 2 μm, 3 μm beads. The error bars, calculated using the error propagation technique, are smaller than the data points and thus omitted in the plot.

IV. DISCUSSIONS

A. Drift velocity

TABLE I. The mean (μ) and standard deviation (σ) of the drift velocity data in Fig. 7

Diameter	$\mu_{x(y)}$ (nm/s)	$\sigma_{x(y)}$ (μm/s)
0.75 μm	9.601 (−62.60)	2.52 (2.48)
2 μm	−11.25 (−15.93)	1.32 (1.29)
3 μm	644.4 (0.147)	1.05 (1.04)

The drift velocities are calculated and tested using Z-test. Other than x-direction in 3 μm results, drift velocities are in the order of nm/s, and considering the displacements of the experiment are in the order of μm, the drifts are significantly small compared to the displacements. However, the drift in the x-direction of 3 μm data is 6.44 μm/s which is comparable to the displacement.

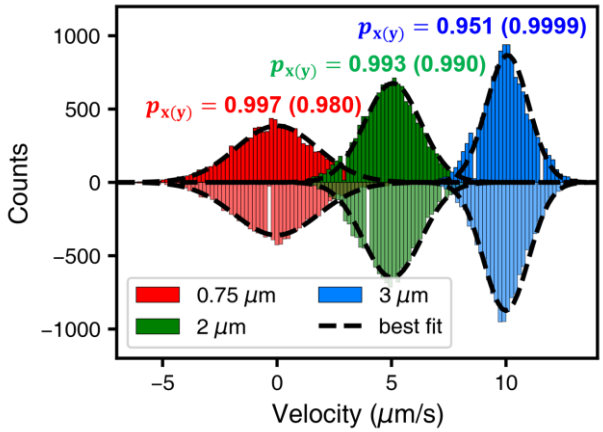

FIG. 9. Histograms of drift velocities in x and y directions. The positive parts represent data for the x-direction, and vice versa. The 0.75, 2, 3 μm data are drawn with offset velocity of 5 μm/s. Counts are fitted with a Gaussian function. p values of Z-test are indicated in the plot.

The number of samples is around 10000 and according to the central limit theorem, the drift velocities are assumed to have a normal distribution and the p-values of the Z-test are well above 0.05 so the null hypothesis H_0: $\boldsymbol{\mu} = 0$ cannot be rejected. However, this assumption holds only for the drift velocities near zero as seen in Q-Q plots in Fig. 11. Data points of high drift velocities deviate from the linear line significantly. It is inferred that this deviation in high velocities comes from the high velocity induced from electrostatic force between beads which is consistent with the results in Fig. 5 (a). Furthermore, from the Gaussian distribution of drift velocities in Fig. 9 the distribution becomes narrow as the radius increases, and the deviations in Q-Q plot also

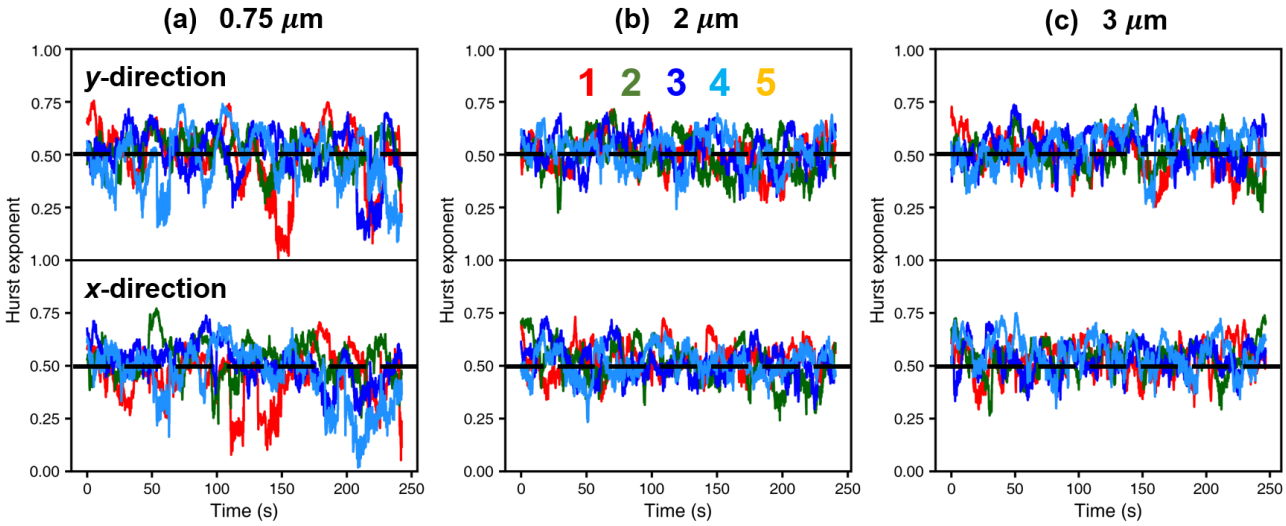

FIG. 10. Hurst exponents (H) of x and y data from Brownian motion data in Fig. 5. The time lag is set to be 10 s. The numbers in (b) indicate the particles in Fig. 5 and dashed lines are for the H = 0.5.

decrease which indicates that the smaller beads suffer from environmental noise or effects that their Brownian motion less likely to be independent.

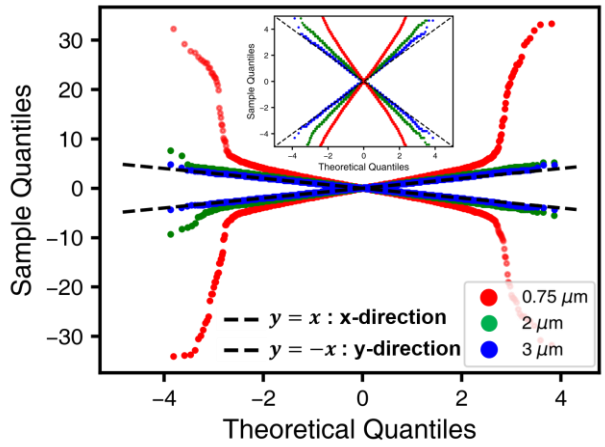

FIG. 11. Q-Q plot of the drift velocity.

B. Trapping force in the Mie regime

According to Eq. 8 in the ray optics regime, the trapping force should increase as the radius increases if the laser power is the same since the refractive index of beads are same in the order of 1.59 ~ 1.60 [5]. However, in the case of 0.75 μm, 2 μm, and 3 μm beads, the radii are close to the 658 nm wavelength of the laser, so neither ray optics nor Rayleigh scattering regimes do not hold. Accurately, ray optics hold when $\frac{2\pi r n_m}{\lambda_0} \gg 1$, where this is 5.729, 15.28, and 22.92 for 0.75 μm, 2 μm, and 3 μm beads. The scattering and gradient force are in between those two regimes that the trapping force increases as radius increases but the detailed dependency is complex, therefore, the balance between the scattering force and the gradient force gets complicated.

C. Validation of Brownian motion – Auto correlation function and Hurst exponent

Ideal Brownian motion is a random process that the increments of trajectory are independent. In other words, the Hurst exponent [7], which is a statistic variable that measures memory of the time series, is equal to 0.5 which represents the memory is short and the autocorrelation decays exponentially in time. The Hurst exponent H ranges from 0 to 1. From 0 to 0.5, the time series has anti-persistent trend that the values exhibit oscillatory motion. For 0.5 to 1, the time series has long term memory that autocorrelation decays slower than exponential which leads to persistent trend in time series data.

The results in Fig. 10 show that the Hurst exponents of the Brownian motion are populated around H = 0.5 but there are significant drops in 0.75 μm data around t = 100 ~ 150 s. From Fig. 5, this time range is also when the displacements deviate from linear regression which again proves that correlated movements occurred at this time.

D. Different types of beams and objects

Here, we used a TEM 00 mode Gaussian laser for trapping beads. Even if the beam has a different shape other than a Gaussian, it can generate gradient force to trap particles. The basic principle of optical trapping is that restoring force is generated when the laser is incident on particles due to the difference in

refractive index. Therefore, in the general case using a Gaussian beam, around the waist of the Gaussian intensity profile, the optical force goes to global maxima or minima and decreases as the displacement goes large. The typical three types of different Gaussian modes and resulting optical trapping forces are calculated using Eq. 6-8 and shown in Fig. 12. Between the global maxima and minima, the particles can be trapped.

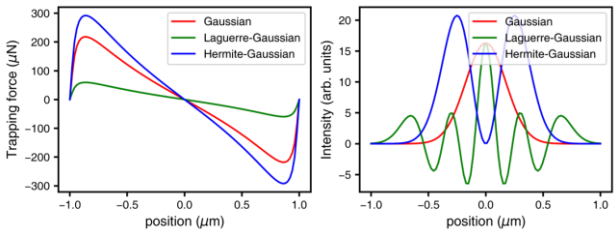

FIG. 12. (left) Optical trapping forces with the Gaussian, Laguerre-Gaussian, and Hermite-Gaussian modes and (right) the intensity profiles. p = 4 for Laguerre polynomial and m, n = 1 for Hermite modes. The refractive index, laser power, particle radius, and beam waist used in the calculation are 1.59, 32 mW, 1 μm, and 0.5 μm.

For objects that have other shapes than a sphere, they can still be trapped by laser. As discussed previously, optical trapping occurs due to the difference in refraction index, an object such as a cube, cylinder, or even a random ellipsoid can be trapped if the laser is well-focused on the particle [8-9]. To make the difference in refractive index, the particle will rotate with respect to the direction of the incident laser and get trapped.

E. Needs of coherent laser

The key aspect of optical trapping using a light source is to be tightly focused on the particle. The light source, typically a laser, should be coherent for generating highly strong and localized gradient force to trap small particles ranging from nanometers to micrometers. Since the gradient force is strongest around the waist of the Gaussian beam. If the light source is incoherent, the gradient force alongside the light cannot be strong enough to trap small particles and the restoring force cannot be symmetrically formed to accurately capture particles [10].

V. CONCLUSIONS

Here, we observed and measured the Brownian motion of polystyrene beads with radii 0.75 μm, 2 μm, and 3 μm. Trapping forces of those beads are measured varying the power of the 658 nm laser. From the analysis, the measured Brownian motions obey the random process mostly while some high velocities induced from drift or electrostatic force by nearby beads affect the overall independence. The trapping force showed good linearity with respect to the power of the input laser which is consistent with the theory. The velocities of the Brownian motion follow the Gaussian distributions well except for the high velocities term. From the Hurst exponents and the trajectories of Brownian motion, the regions where the Hurst exponents are significantly far away from 0.5, the trajectories also showed deviation from the random process which leads to high variations in linear regression.

ACKNOWLEDGEMENTS

The author wants to appreciate our teammates, Juwon Choi, Hyeonsung Jo, and Junyoung Lee for conducting these subtle experiments and having valuable discussions on the analysis of the results. The author would like to also thank to T. A. for allowing early experiment due to the army issue and helping us for the initial measurement setup.

REFERENCES

[1] Stokes GG. On the Effect of the Internal Friction of Fluids on the Motion of Pendulums. In: *Mathematical and Physical Papers*. Cambridge Library Collection - Mathematics. Cambridge University Press; 1-10 (2009).
[2] Thorlab. Portable Optical Tweezers Kit Manual. https://www.thorlabs.de/_sd.cfm?fileName=MTN024417-D02.pdf&partNumber=EDU-OT3. [Online; accessed 25-May 2024].
[3] Thorlab. Kinesis software. https://www.thorlabs.com/newgrouppage9.cfm?objectgroup_id=10285. [Online; accessed 25-May 2024].
[4] Polybead® Sampler Kit I. Technical data sheet 788. https://www.polysciences.com/india/polybead-sampler-kit-i. [Online; accessed 25-May 2024].
[5] Polybead® Sampler Kit I. Technical data sheet 238. https://www.polysciences.com/media/pdf/technical-data-sheets/238-Polystyrene-FAQ.pdf. [Online; accessed 25-May 2024].
[6] Efron, B. in Breakthroughs in Statistics 569–593 (Springer, 1992).
[7] Hurst, Harold Edwin. "Long-term storage capacity of reservoirs." *Transactions of the American society of civil engineers* 116.1 (1951): 770-799.
[8] Herranen, Joonas, et al. "Non-spherical particles in optical tweezers: A numerical solution." *PloS one* 14.12 (2019): e0225773.
[9] Phillips, David B., et al. "Shape-induced force fields in optical trapping." *Nature Photonics* 8.5 (2014): 400-405.
[10] Ashkin, Arthur. "Optical trapping and manipulation of neutral particles using lasers." *Proceedings of the National Academy of Sciences* 94.10 (1997): 4853-4860.